Journal of Materials Chemistry A

Atomistic understanding of structural evolution, ion transport and oxygen stability in layered NaFeO2

Journal:	*Journal of Materials Chemistry A*
Manuscript ID	TA-ART-11-2018-010767.R1
Article Type:	Paper
Date Submitted by the Author:	30-Dec-2018
Complete List of Authors:	Gao, Yurui; California State University Northridge, Wang, Zhaoxiang; Institute of Physics, Chinese Academy of Sciences, Laboratory for Renewable Energy Lu, Gang; California State University Northridge

Journal Name

ARTICLE

Atomistic understanding of structural evolution, ion transport and oxygen stability in layered $NaFeO_2$

Yurui Gao,[a] Zhaoxiang Wang [b,c] and Gang Lu *[a]

Received 00th January 20xx,
Accepted 00th January 20xx

DOI: 10.1039/x0xx00000x

www.rsc.org/

α-$NaFeO_2$ shares a structure similar to many layered electrode materials in Li-ion and Na-ion batteries. In this work, first-principles calculations are carried out to gain atomistic understanding of structural evolution, ion transport and oxygen stability in $NaFeO_2$. Based on the calculation results, we provide an atomistic description of phase transition and structural changes during the charging process. Meanwhile, we identify a di-vacancy assisted diffusion mechanism for Na ions and estimate the diffusion barrier that agrees with experimental data. Furthermore, we reveal that lattice strains could modulate both ion transport and oxygen stability in $NaFeO_2$. A moderate 3% tension in the out-of-plane direction could render the ion diffusion barrierless. Moreover, it is predicted that in-plane compressions can stabilize oxygen and suppress oxygen evolution at high potentials. Thus, a combination of the out-of-plane tension with the in-plane compression is expected to reduce the diffusion barrier and stabilize oxygen simultaneously.

1. Introduction

Recent crisis in energy and environment has prompted intense research and development of renewable energy technologies, among which energy storage is of critical importance. Sodium (Na)-ion batteries (SIBs) are drawing particular attention as potential power sources thanks to the abundance of Na in seawater and the earth's crust. Several common electrode materials in SIBs [1-6] have been studied and their structural resemblance to the electrode materials in Li-ion batteries (LIBs) has been explored. Among them, layered oxides with a formula of A_xMO_2 are of great interest. Here A represents an alkali metal ion and M can be either one or more transition metal ions. Most of this oxide family consists of $(MO_2)_n$ sheets formed by edge-sharing MO_6 octahedrons, between which the alkali ions are inserted or intercalated into an octahedral (O), tetrahedral (T) or prismatic (P) motif of oxygen ions. According to the stacking order of the $(MO_2)_n$ sheets, the layered oxides can be further categorized as O2, O3, and P3 structures, etc. [7]

Among the layered A_xMO_2, α-$NaFeO_2$ is of particular interest because of its low cost, nontoxicity and the fact that it has been widely used as a prototypical model for this class of materials.[8,9] In α-$NaFeO_2$, $(FeO_2)_n$ sheets arrange themselves in the O3 structure with ABCABC stacking. The theoretical specific capacity of $NaFeO_2$ can reach 241 mAh/g by assuming that all the Na ions can be extracted. It has been reported that α-$NaFeO_2$ can deliver a stable and reversible specific capacity of 85 mAh g^{-1} and exhibits a flat voltage plateau at 3.3 V with a charging voltage cutoff of 3.4 V *vs.* Na^+/Na.[10-13] However, its Coulombic efficiency at the first cycle is relatively low and the capacity retention remains unsatisfactory. Moreover, its performance significantly deteriorates when $NaFeO_2$ is charged to a higher voltage above 3.5 V, and the material becomes electrochemically inactive when charged to 4.5 V.[11]

Much progress has been made to elucidate redox reaction mechanism and corresponding structural evolutions in α-$NaFeO_2$. For example, it has been found that $NaFeO_2$ undergoes Fe^{3+}/Fe^{4+} redox reaction during the charge/discharge cycles accompanied by the formation of a monoclinic phase ($Na_{0.5}FeO_2$, C2/m).[12,14,15] Furthermore, Lee[16] *et al.* reported a continuous evolution from the hexagonal O3 ($R\bar{3}m$) to O"3 ($R\bar{3}m$) and to monoclinic C2/m phases during the charge/discharge process. They also revealed that Fe^{4+} species can be spontaneously reduced to Fe^{3+}, in conjunction with the oxidation of the electrolyte, which leads to lowed Coulombic efficiency and increased electrode impedance. More recently, the structural transition from O3 ($R\bar{3}m$) to monoclinic C2/m was confirmed in $NaFeO_2$ by *in situ* X-ray diffraction and its connection to the redox reactions has been examined.[17]

---

[a] Department of Physics and Astronomy, California State University Northridge, Northridge, California 91330-8268, USA. *E-mail: ganglu@csun.edu.

[b] Key Laboratory for Renewable Energy, Chinese Academy of Sciences, Beijing Key Laboratory for New Energy Materials and Devices, Institute of Physics, Chinese Academy of Sciences, Beijing 100190, China.

[c] School of Physical Sciences, University of Chinese Academy of Sciences, Beijing 100190, China.

† Electronic Supplementary Information (ESI) available: See DOI: 10.1039/x0xx00000x

Despite the intense research on $NaFeO_2$ in the past decades, some fundamental questions remain to be answered. For example, the structural evolution at the atomic scale during the charge/discharge process is yet to be elucidated. The atomistic mechanism of ion transport in $NaFeO_2$ has not been established. Oxygen stability at high potentials is crucial to the capacity decay of the electrode, but strategies to stabilize oxygen are still lacking. Although the presence of lattice strain is ubiquitous during the charge/discharge process, its effect on the electrochemical performance of $NaFeO_2$ has not been explored. As well know, theoretical calculations, modeling and simulations can provide insight into fundamental process that are not otherwise accessible, and has become an integral part of material design.[18-22] In this work, we aim to bridge these gaps by first-principles investigations. More specifically, we provide an atomistic scale understanding of the structural evolution during the charge/discharge process. We elucidate the atomistic mechanism by which Na ion transport takes place. The diffusion energy barrier inferred from the proposed mechanism matches the experimental data. We examine how lattice strains could modulate ion transport and oxygen stability in $NaFeO_2$. In particular, we discover that 3% tensile strain in the out-of-plane direction could render the ion transport barrierless, leading to ultrafast rate performance. Furthermore, we predict that the in-plane compressions can stabilize oxygen and suppress oxygen evolution at high potentials.

2. Computational Methodology

Spin-polarized density functional theory (DFT)[23,24] calculations implemented in Vienna *Ab-initio* Simulation Package (VASP) are performed with the projector-augmented-wave pseudopotentials[25,26] and Perdew-Burke-Ernzerhof[27] exchange-correlation functional. Na (3s), Fe (3d, 4s) and O (2s, 2p) orbitals are treated as valence states. The DFT+U approach[28] is used to account for the strongly correlated *d*-electrons in $(FeO_2)_n$. The choice of U is described below. The cutoff energy of plane-wave basis is set at 500 eV. The nudged elastic band (NEB) method[29-31] is used to calculate the diffusion energy barrier of Na ion.

The charging of $NaFeO_2$ is modeled by varying x value in a Na_xFeO_2 supercell. For Na_xFeO_2 in $R\bar{3}m$ structure (Figure 1A) with x = 1 and 0.67, we use a 3×3×1 supercell (27 Na_xFeO_2 units). To model Na_xFeO_2 in C2/m structure (Figure 1B) with x = 0.33 and 0.5, a 2×3×2 supercell (24 Na_xFeO_2 units) is used. For each x, we have to consider all possible arrangements of Na vacancies in Na_xFeO_2 and identify the lowest energy configuration. This configuration represents the ground state structure corresponding to a particular charging state. A Γ-centered *k*-point mesh of 2×2×1 and 2×3×2 is used in the $R\bar{3}m$ and C2/m structure, respectively.

3. Results and discussion

3.1 Calibration of U

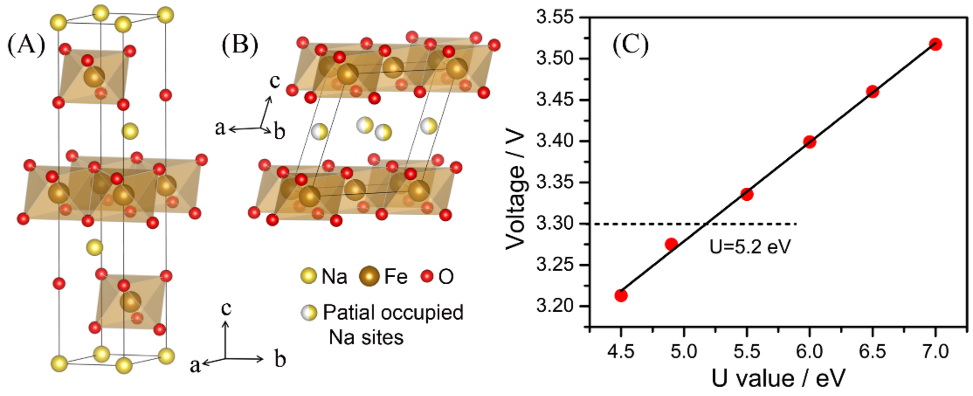

Figure 1. The unit cells of Na_xFeO_2 in $R\bar{3}m$ structure (x>0.5, A) and in C2/m structure (x≤0.5, B); The charging voltage (C) as a function of U in $NaFeO_2$.

In this work, we choose U value according to the desodiation voltage V of $NaFeO_2$, which is calculated as:

$$V = \frac{E(\mathrm{Na}_x\mathrm{FeO}_2) - E(\mathrm{NaFeO}_2) + (1-x)E(\mathrm{Na})}{(1-x)\mathrm{e}} \qquad (1)$$

Here $E(NaFeO_2)$, $E(Na_xFeO_2)$ and $E(Na)$ represent the total energy of $NaFeO_2$, dis-intercalated Na_xFeO_2 and metallic Na, respectively. Because the experimental charging potential exhibits a rather flat plateau for $0.67 < x < 1$,[17] we consider this voltage the most appropriate to calibrate U. More specifically, we choose x = 0.67 in Eq. (1) to calculate the corresponding voltage, which depends on U as shown in **Figure 1C**. With U = 5.2 eV, we obtain V = 3.30 V, which matches the experimental voltage plateau value.[17] Hence U = 5.2 eV will be used in the DFT+U calculations. Note that this U value is comparable to those reported by others for similar oxides.[32,33]

3.2 Diffusion mechanism of Na in $NaFeO_2$

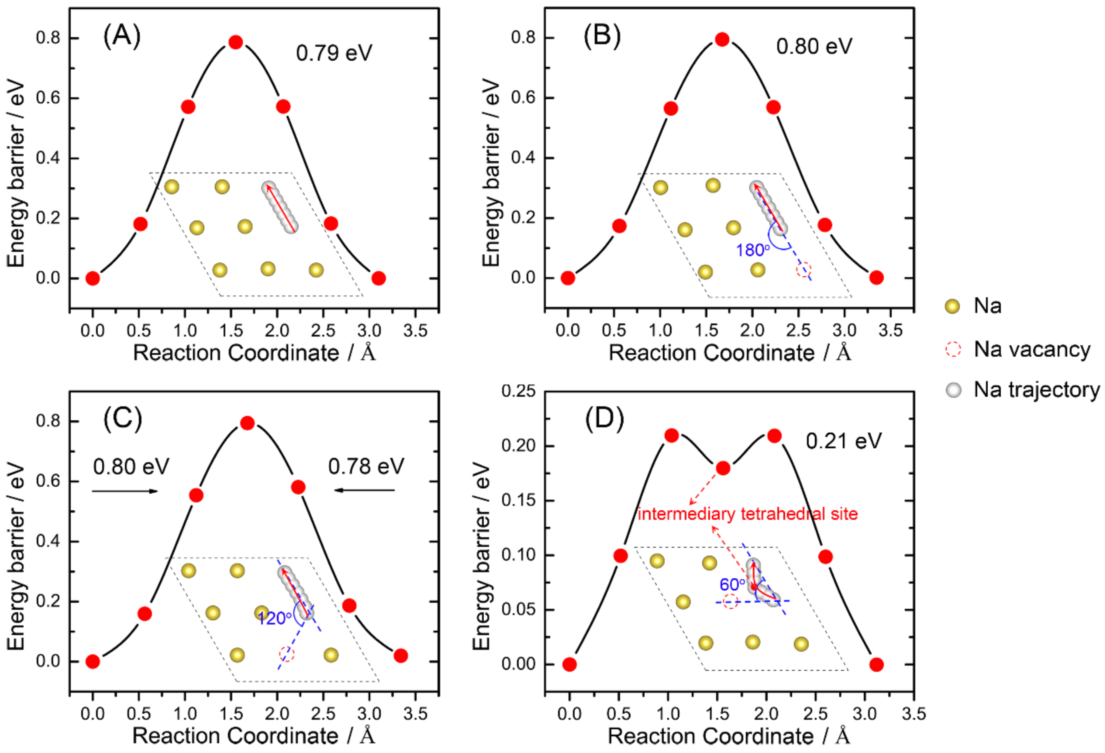

Figure 2. Diffusion energy barrier of Na ion between two adjacent octahedral sites in $NaFeO_2$ without a nearby Na vacancy (A) and with a nearby Na vacancy (B-D). The arrows connecting the two octahedral sites denote the diffusion pathways.

Diffusion mechanism of Na ions is crucial to the rate performance of $NaFeO_2$. As Na ions occupy the octahedral sites in the Na layer, the diffusion energy barriers between two adjacent octahedral sites are calculated to estimate the diffusion kinetics. In all calculations, the final site is assumed to be a Na vacancy. If there is no additional Na vacancy, the diffusion path between the two adjacent sites is found to be a straight-line, and the corresponding energy barrier is 0.79 eV (**Figure 2**A). This value is much higher than the experimental value of 0.31 eV.[15] Therefore, we speculate that additional vacancies may be present in assisting the diffusion of Na ions, as examined next.

We have considered three non-equivalent configurations in which an additional vacancy is introduced at the adjacent octahedral site of the diffusing Na ion, as shown in Figure 3B to D. For the first configuration in **Figure 2B**, the energy barrier (0.80 eV) and the diffusion path are similar to those in **Figure 2A** in the absence of the additional vacancy. For the second configuration shown in **Figure 2C**, we find that the pathway is slightly curved with the similar energy barrier to that in **Figure 2A** and **2B**. For the third configuration in **Figure 2D**, however, the energy barrier drops precipitously to 0.21 eV. The corresponding pathway is curved towards the vacancy via an intermediary tetrahedral site, which is made possible by the presence of the vacancy. This planar octahedral-tetrahedral-octahedral diffusion pathway is similar to the diffusion pathway of A in $A_x(In_xSn_{1-x})O_2$ (A = Na and K) reported by Delmas[34]. This pathway is also similar to the tetrahedral-site-hop mechanism in Li_xCoO_2 proposed by Van der Ven.[35,36] Since this diffusion barrier of 0.21 eV is close to the experimental value[15], the mechanism shown in **Figure 2D** is likely to be operative in $NaFeO_2$. In other words, appropriate amount of Na vacancies is probably beneficial to the rate performance. Furthermore, we can estimate the diffusion coefficient (D) according to the following equation:

$$D = \frac{1}{n} l^2 v_0 exp\left(-\frac{E_a}{k_b T}\right). \qquad (2)$$

Here, n = 4 for the 2D diffusion in layered $NaFeO_2$; l is the hopping distance; E_a is the diffusion barrier (0.21 eV); k_b is the Boltzmann constant, T is the temperature, and v_0 is the characteristic vibration frequency (~10^{13} Hz). With these parameters, we estimate the diffusion coefficient as 4.5×10^{-6} cm^2 s^{-1} at 300 K.

3.3 Structural evolution during desodiation

It is known that during the charging process, $NaFeO_2$ undergoes a phase transition from hexagonal $R\bar{3}m$ phase to monoclinic C2/m phase at half Na extraction. However, the corresponding atomistic structural evolution is not clear. In the following, we carry out first-principles calculations by considering three typical desodiation stages: $Na_{0.5}FeO_2$ (half extraction), and $Na_{0.67}FeO_2$ and $Na_{0.33}FeO_2$ as representatives for less and more than the half extraction, respectively. Hence, $Na_{0.67}FeO_2$ is modeled in the $R\bar{3}m$ structure while $Na_{0.5}FeO_2$ and $Na_{0.33}FeO_2$ in the C2/m structure.

Our goal is to determine the lowest-energy configuration of the three representative stages. To this end, we consider all possible arrangements of Na ions in a single Na layer of Na_xFeO_2. In total, 28, 462 and 330 different configurations of the inner-layer Na ions are considered for x = 0.67, 0.5 and 0.33, respectively, and the lowest energy arrangement of Na ions for each x is identified. Here we assume that each Na layers takes the identical arrangement, which is justified in an ideal and uniform charging condition. Furthermore, we consider the relative shifts between the Na layers for each stage, but find negligible energy difference (~4.5 meV/*f.u.*) between the shifts, owing to the large distances between the layers. The final atomic structures corresponding to the lowest-energy configurations of Na_xFeO_2 (x = 0.67, 0.5 and 0.33) are shown in **Figure 3**. The dashed lines in Figure 3 outline the supercells used in the calculations.

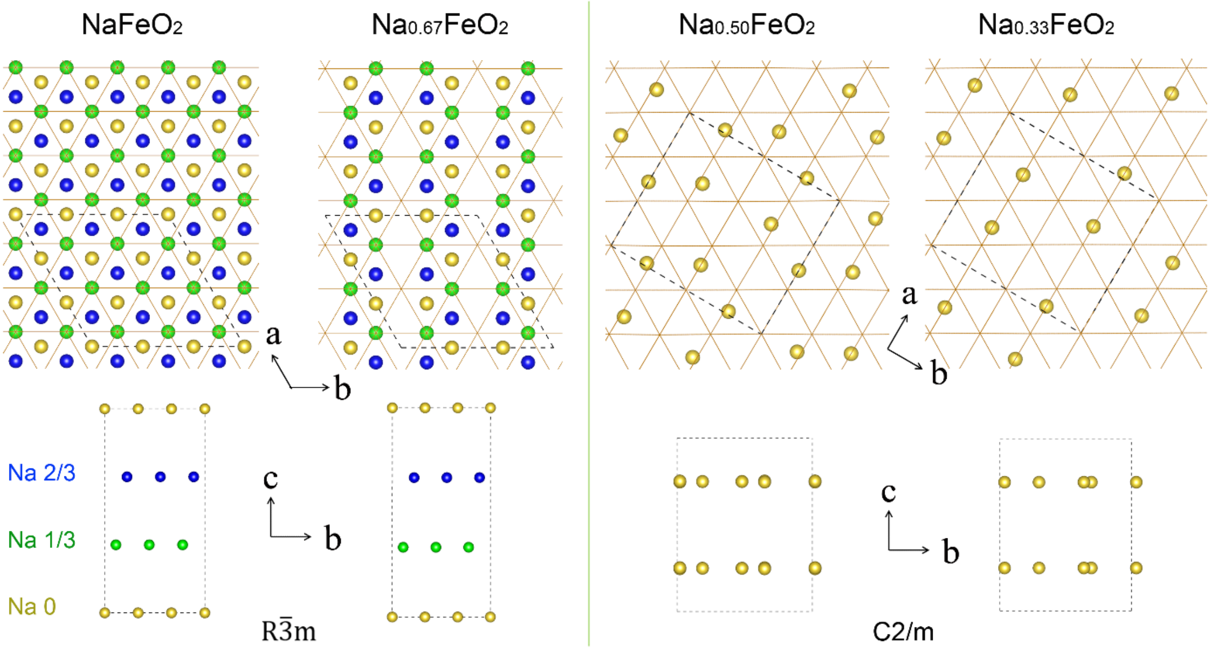

Figure 3. Arrangements of Na ions in the lowest-energy configurations of Na_xFeO_2 (x = 1, 0.67, 0.5 and 0.33) viewed along the c direction (upper panel) and along the a direction (lower panel). Different Na layers in $NaFeO_2$ and $Na_{0.67}FeO_2$ are shown in different colors. Fe and O atoms are not shown for clarity. The vertices of each orange triangle are occupied by Fe ions.

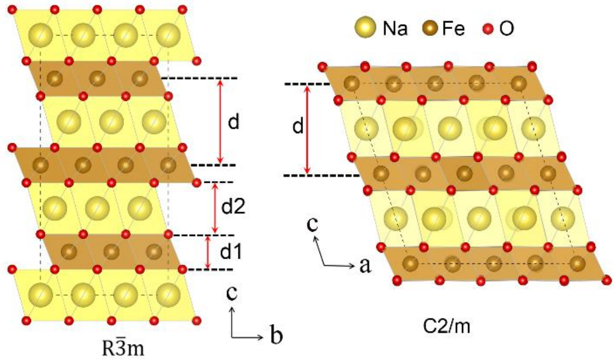

Figure 4. The supercells used in the calculations for the $R\bar{3}m$ structure (left) and C2/m structure (right) for Na_xFeO_2.

In $NaFeO_2$ ($R\bar{3}m$), Na ions arrange themselves uniformly in each layer, occupying the vertices of three sets of translated equilateral triangles. The extraction of 0.33 Na ($Na_{0.67}FeO_2$) involves removing one Na ion in the a and b directions for every three Na ions, forming three sets of shifted hexagons. The resultant pattern of Na ions resembles that of Mn ions in Li_2MnO_3. From $Na_{0.67}FeO_2$ to $Na_{0.5}FeO_2$, the phase transition from the hexagonal ($R\bar{3}m$) to the monoclinic (C2/m) structure takes place, and the remaining Na ions adopt an on-top stacking in the *c*-direction. Further desodiation to $Na_{0.33}FeO_2$ does not yield significantly different structural changes.

We next pay attention to the changes of the structural motifs. As *x* is reduced from 1 to 0.33, we find that the distance between the two adjacent Fe layers (or Na layers), *d*, increases from 5.37 to 5.74 Å (or 7% increase, **Table 1S**) while the area (per Fe ion) in the *ab*-plane shrinks. Moreover, the thickness of the FeO_6 motif (d1) decreases while the thickness of the NaO_6 motif (d2) increases. This is due to the fact that as the positively charged Na ions are extracted, the net repulsion acting on the O layers increases, thus d2 is increased. At the same time, the valence of Fe ions rises from +3 to +4, increasing the attraction between Fe and O ions, thus d1 decreases. We find that the increase in d2 overcompensates the decrease of d1, hence d (= d1 + d2) increases as Na is removed. The “abnormal” volume expansion as Na is removed from $NaFeO_2$ resembles that observed in $NaNbO_2$.[37]

3.4 Effects of lattice strain on ion transport and oxygen stability

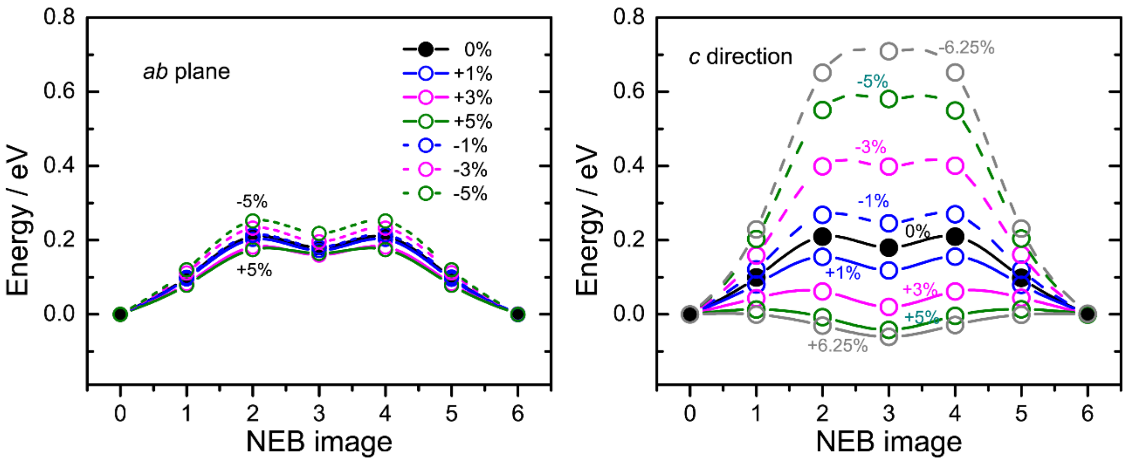

Figure 5. The diffusion energy barrier of Na ions in $NaFeO_2$ in the presence of biaxial strains in the *ab* plane (left) and of the uniaxial strain in the *c*-direction (right). The positive or negative value of strain represents tension or compression, respectively.

In the following, we examine the effect of strains on Na transport in $NaFeO_2$. We apply a uniaxial strain in the *c*-direction ($\varepsilon = \Delta c/c$), ranging from -6.25% (compression) to +6.25% (tension) and a biaxial strain in the *ab*-plane ($\varepsilon = \Delta a/a = \Delta b/b$) from -5% to +5%. Note that the applied strains are not large enough to induce obvious structural transitions in Na_xFeO_2. We have examined the energetics of the sliding of FeO_2 slab in Na_xFeO_2 and found that the O3 stacking structure remains stable under the strains (Figure S1). Moreover, the $R\bar{3}m$ structure at *x* = 1 and 0.67 or the C2/m structure at *x* = 0.5 and 0.33 can be maintained under most strains.

Based on the vacancy-assisted diffusion mechanism shown in Figure 2D, we calculate the diffusion energy barrier in $NaFeO_2$ as a function of the strain using the NEB method (**Figure 5** and **Table 2S**). We find that the in-plane biaxial tension decreases the energy barrier while the compression increases it. However, the magnitude of the changes is rather small, less than 0.04 eV. In contrast, the uniaxial strain in the *c*-direction has a much greater effect on the diffusion energy barrier. The uniaxial tension is found to reduce the energy barrier while the compression increases it. Remarkably, 3% or greater tension in the *c*-direction could render the diffusion barrierless. A close look at the out-of-plane displacement of the structural motifs indicates that most of the tension is localized in the NaO_2 slabs containing the Na vacancies. In other words, the tension is magnified in the slab where the vacancy-assisted diffusion takes place, yielding a much reduced energy barrier.

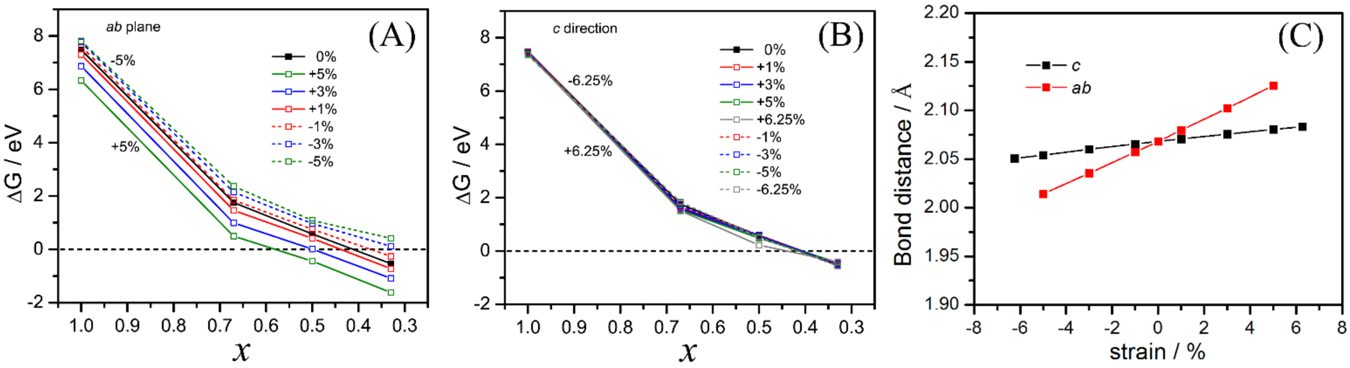

Figure 6. Effect of the biaxial strain in the *ab* plane (A) and the uniaxial strain in the *c*-direction (B) on ΔG for the oxygen evolution reaction: $\mathrm{Na}_x\mathrm{FeO}_2 \rightarrow \mathrm{Na}_x\mathrm{FeO}_{2-\delta} + \frac{\delta}{2}\mathrm{O}_2$. Average Fe-O bond length as a function of the strain (C).

The stability of oxygen during de-intercalation is critical to electrochemical performance, and the instability of oxygen can lead to oxygen release, causing problems such as irreversible structure transition, voltage decay and performance deterioration.[38-40] The instability of oxygen at high charging potentials in $NaFeO_2$ has been observed in our previous work.[17] Here, we extend the previous work and examine the effect of lattice strains on the oxygen stability in $NaFeO_2$ during Na extraction. More specifically, for each applied strain, we calculate the Gibbs free energy change (ΔG) for the following reaction, i.e., O_2 evolution from $NaFeO_2$, at different desodiation stages:

$$\mathrm{Na}_x\mathrm{FeO}_2 \rightarrow \mathrm{Na}_x\mathrm{FeO}_{2-\delta} + \frac{\delta}{2}\mathrm{O}_2. \qquad (3)$$

For Eq. 3, the reaction enthalpy can be calculated according to the following equation:

$$\Delta H = E(\mathrm{Na}_x\mathrm{FeO}_{2-\delta}) + \frac{\delta}{2}E(\mathrm{O}_2) - E(\mathrm{Na}_x\mathrm{FeO}_2) \qquad (4)$$

Here, $E(Na_xFeO_{2-\delta})$, $E(Na_xFeO_2)$ and $E(O_2)$ are the total energy of $Na_xFeO_{2-\delta}$, Na_xFeO_2 and O_2, respectively. The structure of oxygen-deficient $Na_xFeO_{2-\delta}$ is obtained by removing an oxygen atom, which has the least amount of negative charge, from the ground-state configuration of Na_xFeO_2; the structure is then relaxed to compute $E(Na_xFeO_{2-\delta})$. Considering the entropy of O_2 gas at the standard conditions, e.g., $-T\Delta S = -0.63$ eV, 1 bar and 298 K,[41,42] the reaction Gibbs free energy of O_2 release can be estimated. The results of ΔG are shown in Figure 6A and B as a function of the biaxial strain in the *ab*-plane and the uniaxial strain in the *c*-direction. In the absence of strain, as Na is removed from $NaFeO_2$, ΔG decreases, suggesting that oxygen becomes less stable. When ΔG turns negative, the release of O_2 is considered spontaneous. Thus, in the absence of strain, the oxygen evolution is exothermic when $x \leq 0.4$. In the presence of in-plane biaxial strains, we find that compression tends to stabilize oxygen while tension destabilizes it. For example, in the presence of 3% compression, oxygen remains stable as long as $x \leq 0.33$. However, under 3% tension, oxygen becomes unstable as soon as x is less than 0.5. In other words, one can tune the stability of oxygen by the in-plane strains. On the other hand, the uniaxial strains in the *c*-direction are found to have negligible effect on the oxygen stability. To explain the contrasting strain-dependent behaviors, we calculate the average length of Fe-O bonds in $NaFeO_2$ as a function of the strains, shown in Figure 6C. It is found that the average Fe-O bond length depends much more sensitively on the in-plane strains than on the out-of-plane strains. Because the stability of oxygen correlates strongly to the strength of Fe-O bonds, thus the bond lengths, the oxygen stability should also depend more strongly on the in-plane strains than the out-of-plane strains.

Our previous study has revealed that Fe ion tends to migrate into the Na layer in Na_xFeO_2 at a high voltage and when this happens, the Fe ion hinders the transport of Na ions. To examine how strains would affect this behavior, we have calculated the diffusion energy barriers of Na ion under strains in the presence of Fe ion at the Na layer in Na_xFeO_2 ($x = 0.5$ and 0.33). As shown in Figure 2S, we find that the *c*-direction uniaxial tension reduces the diffusion energy barrier of Na while the in-plane biaxial tension increases it. These trends in strain dependence are the same as those in the absence of the Fe ion at the Na layer. However, we note that 3% tension in the *c*-direction could no longer render Na diffusion barrierless. In other words, the strain effect becomes weaker in the presence of Fe ion at the Na layer. Finally, we observe that the presence of Fe ion at the Na layer decreases the oxygen stability substantially, which, however, could be mitigated by strains, such as an in-plane compression or a *c*-direction tension.

4. Conclusions

In summary, we have carried out first-principles calculations to gain atomistic understanding of structural evolution, ion transport and oxygen stability in layered $NaFeO_2$ in the absence and the presence of applied strains. We identify a di-vacancy assisted diffusion mechanism in the NaO_6 slab whose diffusion barrier agrees well to the experimental value. We find that while both the in-plane and out-of-plane strains can modulate the diffusion barrier, the latter has a much greater effect than the former. In particular, we discover that 3% tension in the *c*-direction renders the diffusion barrierless, thus could drastically enhance the rate performance of the electrode. We have examined the structural evolution of $NaFeO_2$ during desodiation and observed an “abnormal” volume expansion as Na ions are removed. Finally, we study the stability of oxygen in the desodiation process and explore how the stability can be tuned by the lattice strains. We reveal that the in-plane compressions can improve oxygen stability while the out-of-plane strains have little effect on it. With a positive Poisson ratio in $NaFeO_2$, a tension in the out-of-plane direction yields a compression in the plane, and vice versa. Therefore, if a sufficient in-plane compression is applied to $NaFeO_2$, it would stabilize oxygen and at the same time lower the diffusion barrier. A possible strategy of applying desirable strains to the oxide is to fabricate thin-film $NaFeO_2$ on a hard or soft substrate. Interfacial strains can be transmitted either passively or actively onto $NaFeO_2$.

Conflicts of interest

There are no conflicts to declare.

Acknowledgements

We thank Dr. Xuefeng Wang and Dr. Yejing Li at University of California San Diego for helpful discussion. This work was supported by the National Science Foundation (DMR-1828019) and the National Key Development Program of China (No. 2015CB251100).

References

1 F. Sauvage, L. Laffont, J.-M. Tarascon and E. Baudrin, *Inorg. Chem.*, 2007, **46**, 3289.
2 D. Kim, E. Lee, M. Slater, W. Lu, S. Rood and C. S. Johnson, *Electrochem. Commun.*, 2012, **18**, 66.
3 H. L. Pan, X. Lu, X. Q. Yu, Y. S. Hu, H. Li, X. Q. Yang and L. Q. Chen, *Adv. Energy Mater.*, 2013, **3**, 1186.
4 S.-M. Oh, S.-T. Myung, J. Hassoun, B. Scrosati and Y.-K. Sun, *Electrochem. Commun.*, 2012, **22**, 149.
5 S. H. Woo, Y. Park, W. Y. Choi, N. S. Choi, S. Nam, B. Park and K. T. Lee, *J. Electrochem. Soc.*, 2012, **159**, A2016.
6 C.-Y. Yu, J.-S. Park, H.-G. Jung, K.-Y. Chung, D. Aurbach, Y.-K. Sun and S.-T. Myung, *Energy Environ. Sci.*, 2015, **8**, 2019.
7 C. Delmas, C. Fouassier and P. Hagenmuller, *Physica B+C*, 1980, **99**, 81.
8 H. Yoshida, N. Yabuuchi and S. Komaba, *Electrochem. Commun.*, 2013, **34**, 60.
9 X. Wang, G. Liu, T. Iwao, M. Okubo and A. Yamada, *J. Phys. Chem. C*, 2014, **118**, 2970.
10 H. Yoshida, N. Yabuuchi and S. Komaba, Na insertion mechanism in Alpha $NaFeO_2$ as positive electrode materials for Na-ion batteries, Honolulu PRiME 2012 ECS Abstr., **2012**, 1850.
11 N. Yabuuchi, H. Yoshida and S. Komaba, *Electrochemistry*, 2012, **80**, 716.
12 J. Zhao, L. Zhao, N. Dimov, S. Okada and T. Nishida, *J. Electrochem. Soc.*, 2013, **160**, A3077.
13 S. Okada, Y. Takahashi, T. Kiyabu, T. Doi, J.-i. Yamaki and T. Nishida, Layered Transition Metal Oxides as Cathodes for Sodium Secondary Battery, 210th ECS Abstr. **2006**, 201.
14 Y. Takeda, K. Nakahara, M. Nishijima, N. Imanishi and O. Yamamoto, *Mater. Res. Bull*, 1994, **29**, 659.
15 M. C. Blesa, E. Moran, C. León, J. Santamaria, J. D. Tornero and N. Menéndez *Solid State Ionics*, 1999, **126**, 81
16 E. Lee, D. E. Brown, E. E. Alp, Y. Ren, J. Lu, J.-J. Woo and C. S. Johnson, *Chem. Mater.*, 2015, **27**, 6755.
17 Y. J. Li, Y. R. Gao, X. F. Wang, X. Shen, Q. Y. Kong, R. C. Yu, G. Lu, Z. X. Wang and L. Q. Chen, *Nano Energy*, 2018, **47**, 519.
18 Z. Shadike, Y. N. Zhou, L. L. Chen, Q. Wu, J. L. Yue, N. Zhang, X. Q. Yang, L. Gu, X. S. Liu, S. Q. Shi and Z. W. Fu, *Nat. Commun.*, 2017, **8**, 566.
19 S. Shi, J. Gao, Y. Liu, Y. Zhao, Q. Wu, W. Ju, C. Ouyang and R. Xiao, *Chin. Phys. B*, 2016, **25**, 018212.
20 P. Hu, X. Wang, J. Ma, Z. Zhang, J. He, X. Wang, S. Shi, G. Cui and L. Chen, *Nano Energy*, 2016, **26**, 382.
21 S. Shi, P. Lu, Z. Liu, Y. Qi, L. G. Hector, Jr., H. Li and S. J. Harris, *J. Am. Chem. Soc.*, 2012, **134**, 15476.
22 S. Shi, H. Zhang, X. Ke, C. Ouyang, M. Lei and L. Chen, *Phys. Lett. A*, 2009, **373**, 4096.
23 P. Hohenberg and W. Kohn, *Phys. Rev.*, 1964, **136**, B864.
24 W. Kohn and L. J. Sham, *Phys. Rev.*, 1965, **140**, A1133.
25 G. Kresse and J. Furthmiiller, *Comp. Mater. Sci.*, 1996, **6**, 15.
26 P. E. Blöchl, *Phys. Rev. B*, 1994, **50**, 17953.
27 J. P. Perdew, K. Burke and M. Ernzerhof, *Phys. Rev. Lett.*, 1996, **77**, 3865.
28 S. L. Dudarev, G. A. Botton, S. Y. Savrasov, C. J. Humphreys and A. P. Sutton, *Phys. Rev. B*, 1998, **57**, 1505.
29 D. Sheppard, P. Xiao, W. Chemelewski, D. D. Johnson and G. Henkelman, *J. Chem. Phys.*, 2012, **136**, 074103.
30 D. Sheppard, R. Terrell and G. Henkelman, *J. Chem. Phys.*, 2008, **128**, 134106.
31 D. Sheppard and G. Henkelman, *J. Comput. Chem.*, 2011, **32**, 1769.

32 F. Zhou, M. Cococcioni, C. A. Marianetti, D. Morgan and G. Ceder, *Phys. Rev. B*, 2004, **70**.
33 W. E. Pickett, S. C. Erwin and E. C. Ethridge, *Phys. Rev. B*, 1998, **58**, 1201.
34 C. Delmas, A. Maazaz, C. Fouassier, J.-M. Réau and P. Hagenmuller, *Mat. Res. Bull.*, 1979, **14**, 329.
35 A. Van der Ven and G. Ceder, *J. Power Sources*, 2001, **97-98**, 529.
36 A. Van der Ven and G. Ceder, *Electrochem. Solid-State Lett.*, 2000, **3**, 301.
37 X. Wang, Y. Gao, X. Shen, Y. Li, Q. Kong, S. Lee, Z. Wang, R. Yu, Y.-S. Hu and L. Chen, *Energy Environ. Sci.*, 2015, **8**, 2753.
38 J.-S. Kim, C. S. Johnson, J. T. Vaughey, M. M. Thackeray, S. A. Hackney, W. Yoon and C. P. Grey, *Chem. Mater.*, 2004, **16**, 1996.
39 D. Y. W. Yu, K. Yanagida, Y. Kato and H. Nakamura, *J. Electrochem. Soc.*, 2009, **156**, A417.
40 Y. Koyama, I. Tanaka, M. Nagao and R. Kanno, *J. Power Sources*, 2009, **189**, 798.
41 J. S. Hummelshoj, J. Blomqvist, S. Datta, T. Vegge, J. Rossmeisl, K. S. Thygesen, A. C. Luntz, K. W. Jacobsen and J. K. Norskov, *J. Chem. Phys.*, 2010, **132**, 071101.
42 P. Atkins and J. de Paula, *Physical Chemistry*, 7th Ed. (Oxford University Press, Oxford, 2002)

TOC Graphical Abstract for:

Atomistic understanding of structural evolution, ion transport and oxygen stability in layered $NaFeO_2$

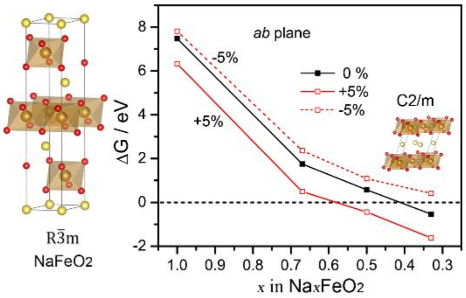

We provide atomistic understanding of structural evolution, ion transport and oxygen stability in layered $NaFeO_2$, and reveal how strains can be used to enhance ion transport and oxygen stability.